31st Congress of the International Council of the Aeronautical Sciences

Belo Horizonte, Brazil; September 09-14, 2018

SYSTEM-LEVEL ASSESSMENT OF TAIL-MOUNTED PROPELLERS FOR REGIONAL AIRCRAFT

Roelof Vos* **and Maurice F. M. Hoogreef***

***Delft University of Technology, Faculty of Aerospace Engineering, Delft, The Netherlands**

Keywords: *Aircraft Design, Propulsion Integration, Ducted Propellers, Technology Assessment*

Abstract

Three regional transport aircraft of different configuration are synthesized for the same design specification using an automated design routine. The first aircraft features wing-mounted propellers, the second aircraft features propellers mounted on the horizontal tail plane, while the last configuration replaces the horizontal and vertical tail with two ducted propellers mounted near the rear of the fuselage. These last two innovative configurations have the potential to reduce the cabin noise, while the ducted propeller could also reduce community noise. The analysis and design methods to size and analyze these configurations include weight and balance, stability and control, aerodynamic performance, and mission performance. Propeller slipstream effects are taken into account and demonstrated to play an important role in the sizing of the horizontal tail surface. A comparison study between the three aircraft for a harmonic mission of 1530km and 7500kg payload demonstrates that the aircraft with wing-mounted propellers has the lowest maximum take-off mass and burns the least amount of fuel. The two innovative configurations have slightly less performance, which is ultimately attributed to the large center-of-gravity excursion that stems from an aft-mounted propulsion system. A 3% increase in maximum take-off weight is predicted along with a fuel burn increase between 5% and 10% for the innovative configurations, respectively. Further investigation of the underlying assumptions might improve these results in future studies.

1 Introduction

This paper presents the conceptual design and assessment of two innovative aircraft configurations that rely on tail-mounted propellers and fuselage-mounted, ducted propellers, respectively. By positioning the propellers further behind the main cabin of the aircraft, the cabin noise stemming from the propeller and the turboshaft engine can be substantially reduced increasing the level of comfort of the passengers. This configuration was already proposed in the 1980s [3] and is currently being investigated in the Clean Sky 2 project called IRON [5]. While the tail-mounted propellers reduce the cabin noise, the flyover and sideline noise hardly change. As a matter of fact, care must be taken when installing the propeller to prevent additional noise stemming from the wing vortex sheet entering the propeller disk at elevated angles of attack and low flap settings. To reduce the community noise, the second innovative configuration shields the propeller with a cowling. This cowling (sometimes termed “duct” or “ring wing”) replaces the vertical and horizontal tail planes and therefore has a synergistic effect: it should reduce the community noise, it should improve the propulsive efficiency, and it should provide sufficient stability and control authority over the entire center-of-gravity excursion. To demonstrate that the configuration with a ducted propeller is feasible a flight test on a subscale model was performed in 2016 (see Fig. 1).

While the flight test was successful and the aircraft demonstrated excellent handling qualities

Fig. 1 Subscale test article of aircraft with fuselage-mounted ducted propellers prior to demonstration flight.

during powered flight, it left the question open whether such an innovative configuration would also improve the fuel burn of the aircraft compared to a more conventional, high-wing aircraft with its propellers mounted on the wing. Therefore, this paper presents a system level assessment of three regional aircraft that are each designed for the same mission requirements but have a different propulsion-airframe configuration. The main objective is to find out what the difference is between these aircraft configurations is in terms of their weight and balance, their aerodynamic performance, and their mission performance.

The following sections will describe the methodology that is followed to design these aircraft (Sec. 2), the top-level aircraft requirements and assumptions (Sec. 3), and a discussion of the results (Sec. 4).

2 Methodology

The conceptual designs of the aircraft are made using the Aircraft Design Initiator (termed the Initiator). The process flow of the Initiator is shown schematically in Figure 2. On the diagonal, the various modules of the Initiator are shown (grey boxes), while the white boxes indicate the variables that serve as output and/or input to the various modules. The large blue arrows indicate the feed forward and feedback directions, while the three colored square perimeters mark the three (partially nested) convergence loops that are present in the Initiator. It should be noted that the variables that are presented here often represent an umbrella for a set of variables. For example, "Fuselage geometry" includes variables on the fuselage cross section, length, upsweep angle, etc. Furthermore, it should also be noted that the synthesis process is a process of convergence, where the design variables are altered in an iterative way until a predefined set of performance indicators converge below a certain threshold within a large set of constraints. In other words, the Initiator uses a process of design ”feasilization” [8], rather than optimization to get a converged aircraft design.

Figure 2 only shows the process flow on an aggregated level. Many of the blocks on the diagonal line contain multiple design, analysis or sizing modules. For example, "Geometry Modules" contains more than 20 individual modules that dimension the aircraft geometry, ranging from engine position to wing taper ratio. Other modules are not listed in Figure 2 such as the sizing modules to determine the horizontal tail or vertical tail area. More information on the process flow of the Initiator can be found in Ref. [2]

For the design of aircraft with (ducted) tail-mounted propellers, particular modifications were made to the stability and control module as well as to the weight and balance module. These are described in more detail in the subsection below. The propeller slipstream effects on lift and pitching moment were included according to the method of Obert, described in Ref. [1].

2.1 Weight Estimation Ducted Propellers

As the weight estimation of the propulsion system plays a pivotal role in the assessment of the various calculations, an overview of these equations is presented here. All masses are computed in pounds (lbs). The engine is integrated in the nacelle, which is connected to the fuselage by means of a pylon. The total nacelle mass, including the pylon, consists of three components: the centerbody (cb) around the turboshaft engine, the

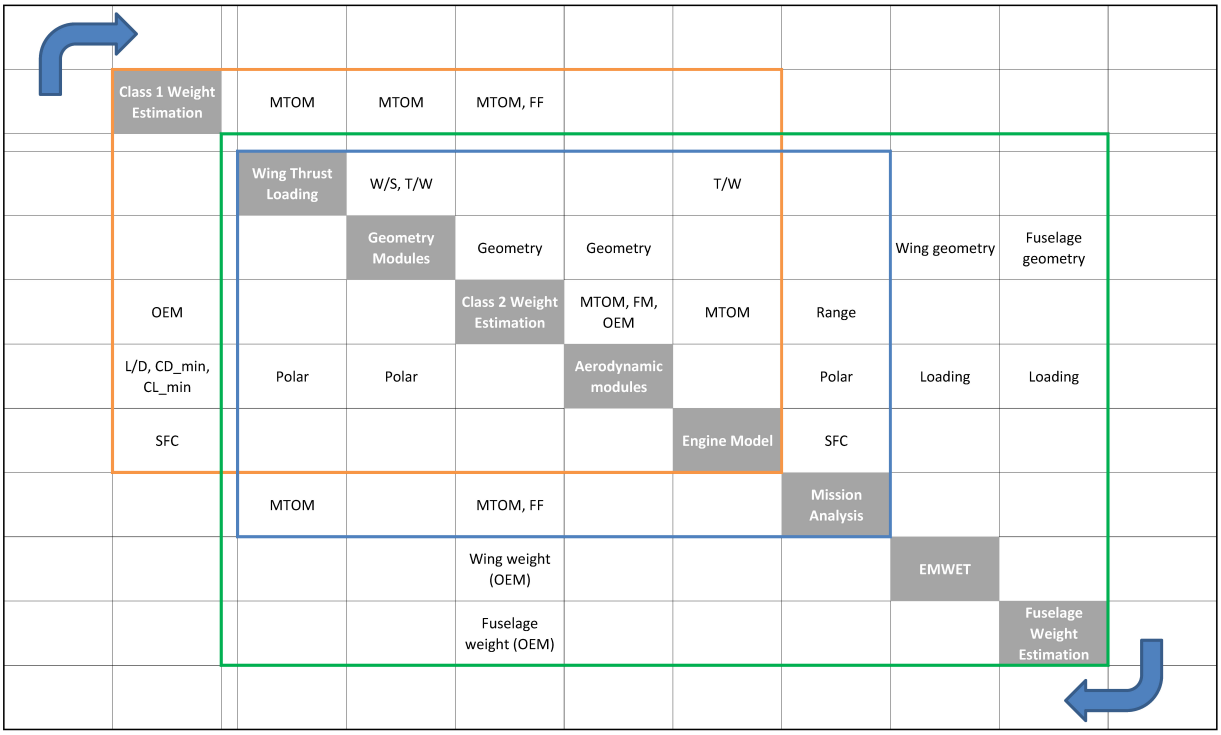

Fig. 2 Design Structure Matrix of the Initiator process flow. On the diagonal the main modules are shown, while on the off-diagonal cells the input/output of modules is displayed. The colored boxes indicate the three nested loops that the initiator executes iteratively.

duct around the propeller, and the pylon:

$$m_{\text{nac}} = m_{\text{cb}} + m_{\text{duct}} + m_{\text{pylon}} \tag{1}$$

The centerbody around the turboshaft engine is computed according to:

$$m_{\text{cb}} = 0.14 W_{\text{TO}} \tag{2}$$

The duct mass is computed according to the nacelle formula for turbofans provided by Raymer [6] assuming 60% of the nacelle mass can be attributed to the duct:

$$m_{\text{duct}} = 0.40 \frac{l_{\text{duct}}^{0.1} w_{\text{duct}}^{0.294} n_{\text{lim}}^{0.119} m_{\text{ps}}^{0.611} N_{\text{en}}^{0.984} S_{\text{duct}}}{N_{\text{en}}} \tag{3}$$

where l_{duct} and w_{duct} are the length and width of the duct (both in ft), respectively, n_{lim} is the ultimate load factor, N_{en} is the number of engines, and S_{nac} is the duct outer surface area in ft^2. The ducted propellers are connected to the fuselage by means of pylons. To estimate their mass, the estimation from Torenbeek [9] for horizontal tail planes has been used assuming they are fixed and that they have no sweep:

$$m_{\text{pylon}} = S_{\text{pylon}} \left(3.81 S_{\text{pylon}}^{0.2} V_D - 0.287 \right) \tag{4}$$

where, V_D is the dive speed in kts, S_{pylon} is the planform area of the pylon in ft^2.

2.2 Aerodynamics of Ducted Propellers

Aerodynamic analyses for the ducted propeller in power-on and power-off conditions were derived from wind tunnel tests performed in the low-turbulence tunnel of TU Delft and reported in the MSc thesis of Harinarain.[4] The reference area that was chosen for the coefficients reported in this subsection equals the projected area of the two ducts onto a horizontal plane:

$$S_{\text{duct, ref}} = \frac{2D}{AR_{\text{duct}}} \tag{5}$$

where D is the duct diameter, and AR_{duct} is the aspect ratio of the duct (D/c), which is a design choice.

The maximum lift coefficient, C_{L_h} of the duct when the propellers were not turning was found in the wind tunnel tests to be to 1. When deflecting the internal control surfaces, an increase in maximum power-off maximum lift coefficient of 20% was found. Furthermore, at a propeller advance ratio of 0.28 and 0.42 the maximum lift coefficient was measured to be 5.1 and 2.5, respectively without any control surface deflection. Based on these results, this study assumes an unpowered maximum lift coefficient of $C_{L_h} = 1.2$ and a (conservative) $C_{L_h} = 3$ for maximum power conditions.

For the angle-of-attack derivative, C_{L_α}, first the power-off lift-curve slope is computed based on the ring-wing (rw) model of Weissinger [10]:

$$C_{L_\alpha}|_{\text{rw}} = \frac{\pi}{2}\zeta c_{l_\alpha} \tag{6}$$

where c_{l_α} is the lift-curve slope of the airfoil used in the ring wing and ζ is computed as follows:

$$\zeta = \frac{1}{a + \lambda\frac{\pi}{2} + \lambda\tan^{-1}(1.2\lambda)} \tag{7}$$

where $\lambda = 1/AR_{\text{duct}}$. The lift-curve slope of the ducted propeller system increases when thrust is applied according to the following formula:

$$C_{L_\alpha} = C_{L_\alpha}|_{\text{rw}}(1 + k_T T_c) \tag{8}$$

where T_c is the thrust coefficient of the propeller with respect to the projected area of a single duct and k_T is multiplication factor that was found to be 0.2 [4].

3 Design Specifications

To assess the effect of tail-mounted propulsion on the aircraft performance, the aircraft are designed according to the top-level aircraft requirements (TLARs) that are stated in Table 1. These requirements are similar to the specifications of an ATR-72-600, which serves as a reference aircraft in this study.

Apart from the TLARs, the Initiator uses many requirements on performance, stability and control, and geometric clearances that stem from the certification specifications (CS-25), the military specifications (MIL-F-8785), or handbooks [7]. The harmonic mission profile, for which the aircraft is sized, consists of the following phases: engine start and warm-up, taxi, take-off at sea level, climb and accelerate to cruise altitude and cruise speed, cruise at constant Mach number and altitude, decent and decelerate to sea level and approach speed, climb to 3300m and travel 100 km (diversion), decent to 1300m, loiter for 30 minutes at 1300m, decent to sea level, land and taxi out. To be able to fly over a longer range with less payload it is assumed that a fuel tank is present between the front and rear spars of each wing half, spanning 80% of the semi-span, starting at the wing symmetry plane.

Table 1 TLARs for regional aircraft design.

Spec.	Unit	Value
Range	km	1530
Structural payload	kg	7500
Pax	-	68
Cruise altitude	m	7000
Cruise Mach	-	0.45
Time to climb to 5400m	min.	17.5

Each aircraft is sized with a constant aspect ratio of 12. Each passenger is assumed to have a mass of 80kg and to carry 22kg of luggage. The remaining payload mass (564kg) is assumed to be additional cargo. All luggage and cargo are assumed to be stowed below the passenger cabin as bulk. The passengers are seated in a 2-2 configuration with a single aisle and a 26 inch seat pitch. Each aircraft is assumed to be equipped with high-lift devices that can increase the (unpowered) maximum lift coefficient to $C_{L_{\max}} = 3.2$. Furthermore, a thrust-specific fuel consumption based on the cruise thrust is assumed of 14.5g/kN/s and a constant propeller efficiency of 80% is assumed for cruise, 65% for take-off and 75% for climb. Furthermore, the induced thrust stemming from the lip suction of the engine cowling (if present) is neglected in the computations.

4 Results

Using the TLARs from Section 3 and the methodology of Section 2, three aircraft were synthesized using the Initiator: 1) a high-wing, T-tailed aircraft with wing-mounted propellers (WMP), 2) a low-wing aircraft with propellers mounted on the tips of the horizontal tail plane (TMP), and 3) a low-wing aircraft with fuselage-mounted ducted propellers (FMDP). The three-views of these synthesized aircraft designs are shown to-scale in Figure 3. From these figures it can be observed that the fuselage of each aircraft has the same outer mold line (OML), while the wings of the two aircraft with aft-mounted propulsions systems have a slightly larger wing, which is shifted further aft on the fuselage. Also the undercarriage of these aircraft is further aft and attached to the wing, making the need for a fuselage fairing obsolete. From the front view it can also be seen that the number of propeller blades varies between the three different configurations, although this had only a very minor effect on the overall results.

4.1 Wing Loading and Power Loading

As the Initiator sizes the aircraft by selecting a design point with the highest wing loading and at that wing loading the highest power loading, it is useful to inspect the wing-loading versus power-loading diagram displayed in Figure 4. Only the constraints that actively bound the design space are shown, omitting the constraints for second-segment climb gradient, time-to-climb, and buffet-onset, which are not active. It can be seen that the take-off field length, the one-engine-inoperative climb gradient requirement in landing configuration, and the landing distance are the requirements that size each of these aircraft. It can also be seen that the cruise constraint is quite different for all three configurations. This is due to the difference in the untrimmed drag polars between the three configurations as will be elaborated below. The wing loading of the WMP, TMP, and FMDP is 3330, 3340, and 3350 N/m^2, respectfully, while the power loading is 66.7, 64.6, and 63.0 N/kW, respectively. This means that although the design point for each aircraft is virtually the same for each of the aircraft in terms of power loading and wing loading, the amount of cruise excess power is highest for the WMP and lowest for the FMDP configuration.

4.2 Weight and Balance

The weight distribution of the three empty aircraft is schematically shown in Figure 5. The location of heavy components such as pressure bulkheads, undercarriage, APU and engines can clearly be discerned. Note that the engine location is visibly different between the three different aircraft configurations, placing a large mass at the tail of the aircraft for the TMP and the FMDP. The coinciding circles at the engine location are indicative of the engine mass, the cowling mass and the engine system mass. While the dry engine mass for both the TMP and the FMDP are both 600kg, the cowling (or duct) of the FDMP is estimated to add 200kg to the installed engine weight. This is still less than the estimated 470kg of the vertical and horizontal tail plane weight of the WMP aircraft. It should be stressed, that the weight of the duct is merely an estimate as no reference data is available on the structural weight of ring wings or propeller ducts.

As the Initiator positions the wing such that the lowest horizontal tail plane area results, each aircraft has a different wing position. The resulting CG excursions for each of the aircraft with respect to their respective mean aerodynamic chords are shown as a function of the loading in Figure 6. These loading diagrams show three lobes for each aircraft. The lowest two lobes can be attributed to the loading of the passengers in window seats and aisle seats. The upper lobe is for the luggage and cargo. It can be seen that the WMP aircraft is assumed to have a single cargo bay below the main passenger floor and therefore its loading diagram looks different from the low-winged configurations that are assumed to have a forward and aft cargo bay, separated by the center wing box.The two ascending lines represent the CG shift resulting from fuel

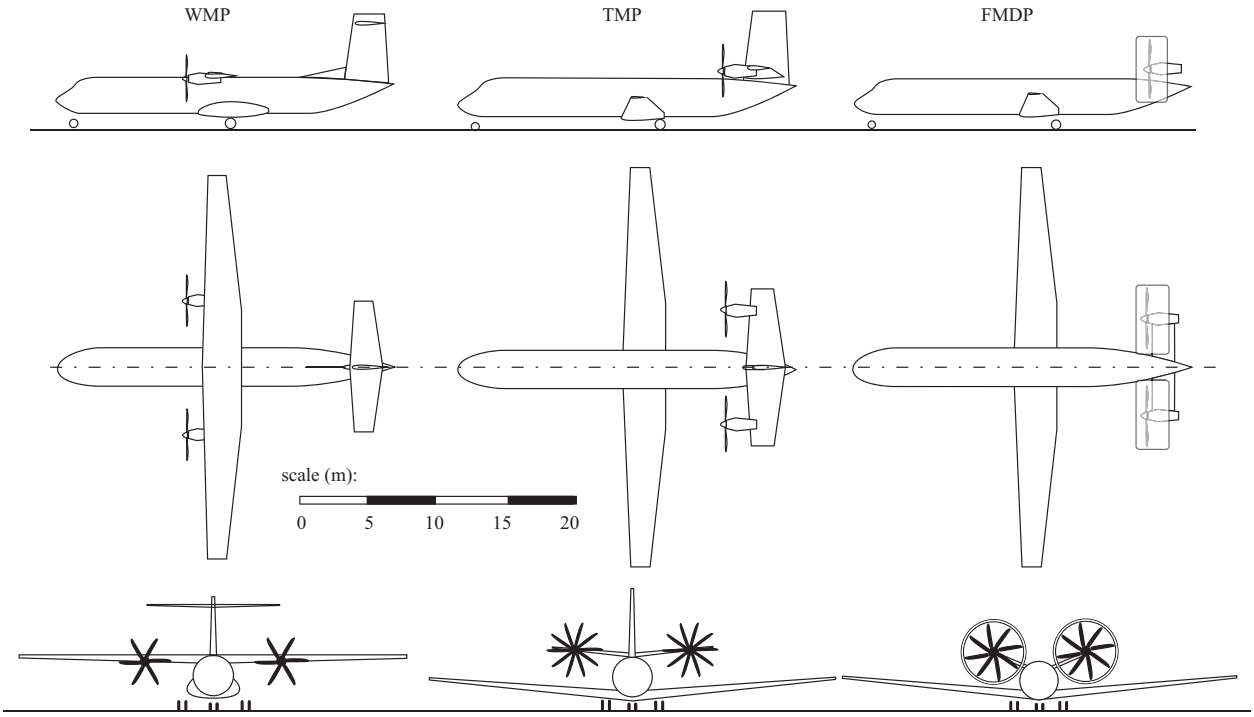

Fig. 3 Three-views of the three synthesized aircraft designs: a conventional aircraft with wing-mounted propellers (WMP, left), a low-wing aircraft with tail-mounted propellers (TMP, center), and a low-wing aircraft with fuselage-mounted ducted propellers (FMDP, right).

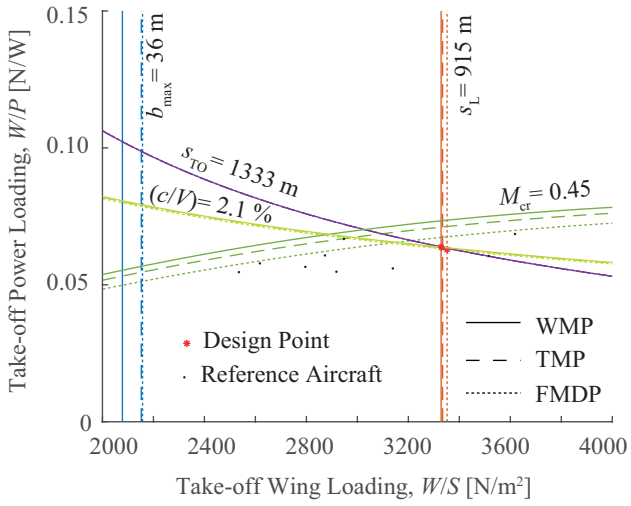

Fig. 4 Wing-loading versus power-loading diagram for each of the three synthesized aircraft configurations.

burn in the case of the harmonic mission (left) and the ferry mission (right). Also the bounds of the CG diagram are indicated as vertical lines intersecting with the horizontal axis of the diagram.

From Figure 6 it can be observed that the loading diagram of the WMP aircraft is quite favorable. The total center of gravity (CG) excursion measures 30% of the MAC, while for the TMP and the FMDP it measures 40% and 41%, respectively. Furthermore, the CG diagram of the WMP aircraft is much less skewed, which keeps the CG around the 25% meaning that little trim drag is to be expected from this configuration. The TMP and FMDP aircraft have their quarter-chord points of the MAC at 49.2% and 52.2% of the fuselage length, respectively. This results in a fairly skewed CG shift with for both aircraft. The reason for this is the large propulsion system mass that is located relatively far behind the wing. To balance and stabilize the aircraft, the wing therefore shifts further aft and the operating empty mass (OEM) CG is found at approximately 54% and 47% of their respective mean aerodynamic chords (MACs). During loading of passengers the CG consequently shifts forward resulting in a total CG excursion of $0.41\bar{c}$ and $0.40\bar{c}$ for the TMP and FMDF, respectively.

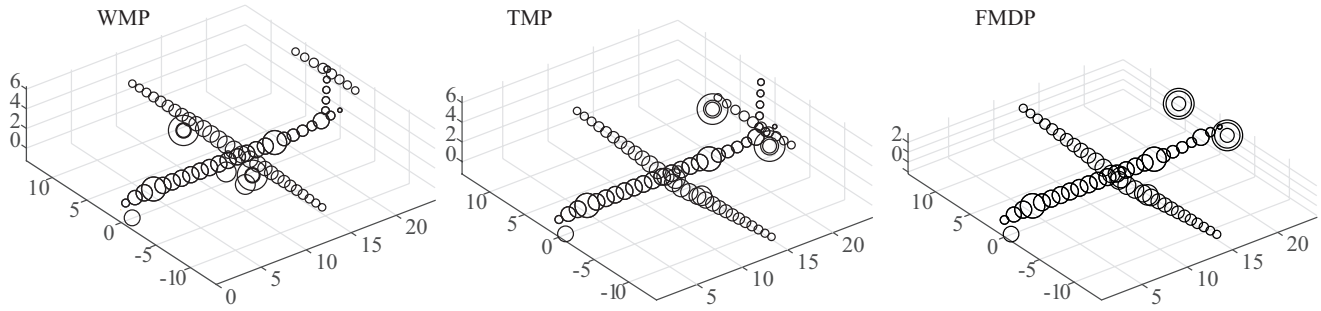

Fig. 5 Distribution of mass over the aircraft. Each circle represents a point mass where the area of the circle is representative of the mass of the individual components.

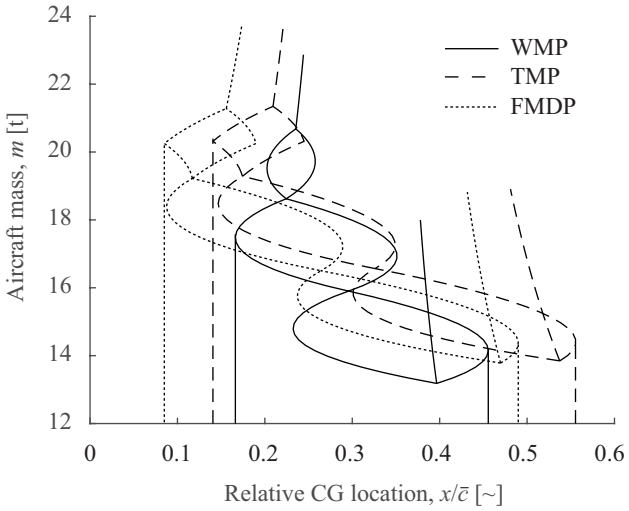

Fig. 6 Loading diagrams of the three different aircraft configurations.

4.3 Stability and Control

Figure 7 shows all the constraints that relate the tail area ratio (S_h/S) to requirements on balance and stability. If we look at the WMP aircraft we can see that the sizing requirements are the power-off equilibrium in landing condition at most forward CG, i.e. pitch-up to $C_{L_{max}}$, and the power-on stability in take-off configuration at most aft CG. The effect of the propeller and its slipstream causes a destabilizing tail-off pitching moment derivative. As the T-tail is not in the slipstream of the propeller, its effectiveness is not influenced by the power of the propeller. This results in a slightly larger tail area ratio of 28% compared to the scenario where propeller slipstream effects are neglected. It can also be seen that, while not sizing, the take-off rotation constraint and the power-on pitch up constraints are also close to the feasible design space. This is because the slipstream effect in power-on conditions generates a relatively large nose-down pitching about the main gear wheel axle and forward center-of gravity, respectively.

If we examine the scissor plot of the TMP (lower left in Fig. 7), it can be seen that the power-on constraint lines on the equilibrium side of the plot are all absent. Even though, these constraints were evaluated, they fall outside the range of the curve to the increased effectiveness of the horizontal tail plane in power-on conditions. Rotation during take-off, or pitch-up to $C_{L_{max}}$ could therefore be satisfied with a much smaller tail, provided the power would always be on. As this is not the case, the tail surface is merely sized for power-off conditions. With the required CG shift of 41%, this results in tail area ratio of 37%, which are lower than the 42% that was found my Goldsmith in his study into this configuration as alternative to the DC-9 [3] but larger than the 35% assumed by Nicolosi et al. for a 130-seat aircraft with the same configuration [5].

The stability plot of the FMDP shows that the horizontal tail area ratio should be 31%. The horizontal tail area for this aircraft is defined as the sum of the projected areas of the two ducts onto the XY plane. The required tail size therefore effectively sizes the diameter of the duct, assuming a duct aspect ratio (D/c) of 2. It can be seen that the tail is sized for power-off con-

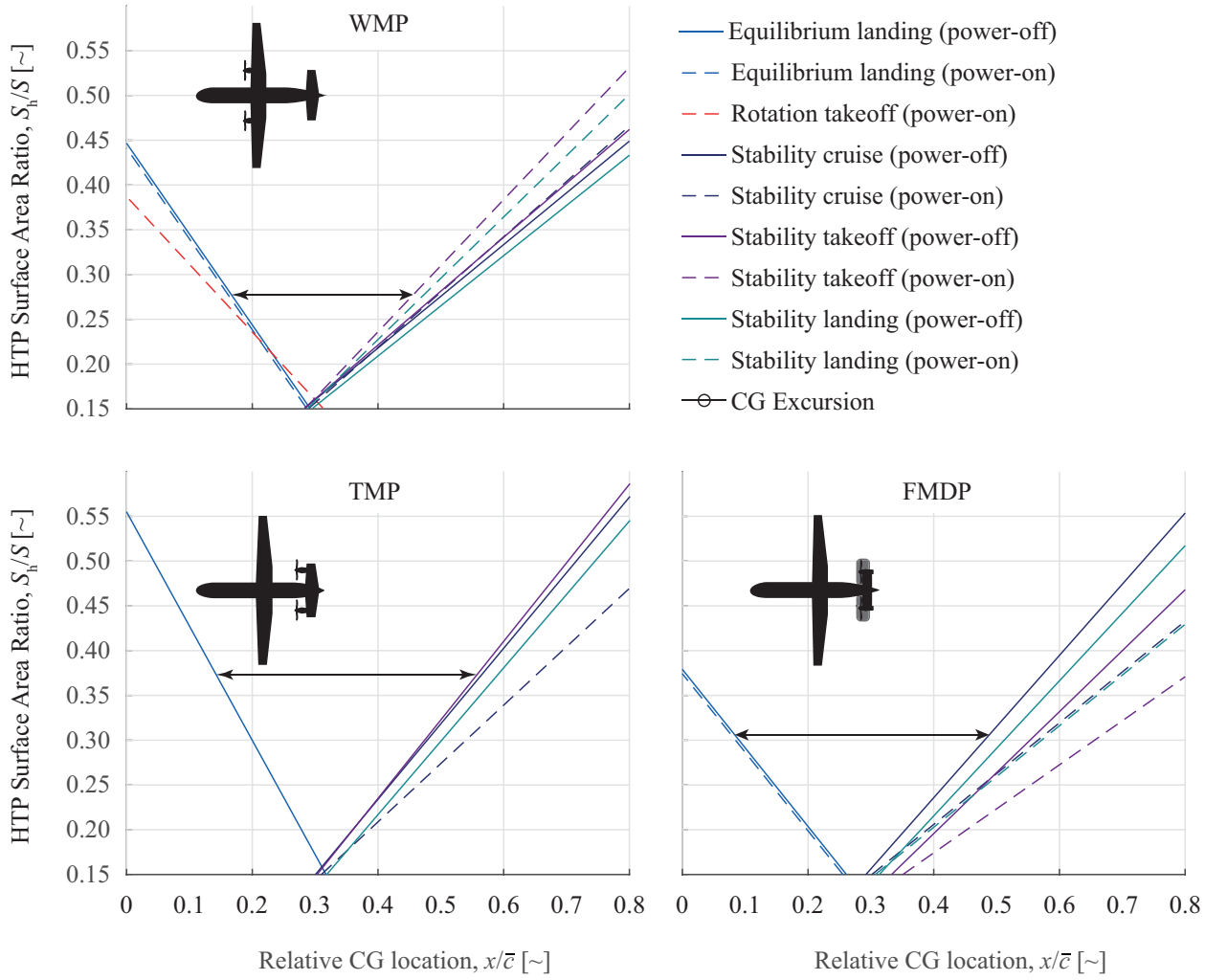

Fig. 7 Scissor plots demonstrating compliance with stability and balance requirements for each aircraft configuration. The arrows show the CG excursion for each aircraft configuration.

ditions, which is to be expected as the tail effectiveness increases with increasing propulsive power. This increases both the maximum lift coefficient of the ducts and their lift-curve slope. When no power is present, the ducts act as ring wings which are consequently sized to meet all constraints on balance and stability. The resulting dimensions of the duct (including structural thickness) are an outer diameter of 5.0m and a chord length of 3.3m. The propeller that is fitted in the ring wing has a resulting diameter of 4.6m. A redesign of this aircraft might favor a duct with a smaller aspect ratio to reduce the propeller diameter and improve the noise shielding capability of the duct.

4.4 Aerodynamic Performance

The aerodynamic performance of the three different aircraft configurations is shown in Figure 8. For each polar, a straight line has been added that originates at the origin and is tangent to the drag curve. The tangency point shows the lift coefficient for which the highest aerodynamic efficiency can be obtained. It can be seen that all three drag polars have approximately the same shape, which is to be expected as they all have the same aspect ratio, wing incidence and fuselage. However, it can also be seen that the WMP has the lowest minimum drag value of 211 counts, while the TMP and FMDP have 219cts, and 235cts, respectively. Note also that the wing area

(and therefore reference area) of each of the aircraft is different and measures 68.1m^2, 70.7m^2, and 70.5m^2 for the WMP, TMP, and FMDP, respectively. For the TMP and the FMDP, the increase in minimum drag coefficient, combined with the larger reference area therefore results in an even higher increase in drag during cruise compared to the WMP.

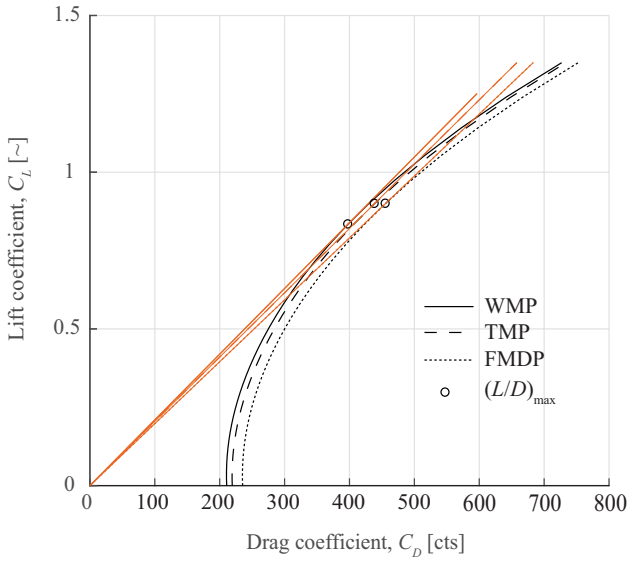

Fig. 8 Drag polars of the three different aircraft configurations at $M = 0.45$.

For the TMP, the increase is attributed to the larger HTP and VTP that result from the aft-mounted engine. The total wetted area of the HTP plus VTP increases from 66m^2 (WMP) to 86m^2 (TMP). For the FMDP, the large increase in minimum drag coefficient is also attributed to the friction drag of the propeller ducts. Because it is assumed that both the outside and inside of the ring wings contribute to the friction drag coefficient, the total wetted area of the two ring wings adds up to 205m^2, which is more than double the wetted area of the TMP and triple the wetted area of the WMP. In practice, it is anticipated that part of this friction drag is offset by an increased lip suction over the ring wing that is present when the propellers provide thrust as shown by Harinarain [4]. However, this has not been considered in the present study.

Finally, one can conclude from the drag polars of Fig. 8 that the optimum cruise lift coefficient for maximum L/D is around 0.8 for each of these aircraft. At the set cruise altitude of 7000m, each of these aircraft cruise at a lift coefficient of 0.57, which is below their predicted optimum.

4.5 Mission Performance

The conventional aircraft with wing-mounted engines is very similar to the ATR-72-600. In fact, its estimated maximum take-off mass (22870kg) is close to the reference value (22800kg). Also, the operating empty mass is relatively close (13200kg versus 13300kg, respectively). While the wing loading is 11% lower than the reference value (3330 N/m^2 versus 3670N/m^2, respectively), the power loading is 5% higher (0.064N/W versus 0.061N/W, respectively). This indicates that the assumed maximum lift coefficient in landing condition ($C_{L_{\max}} = 3.2$) is slightly underestimated. The length of the fuselage measures 24.8 meters, which is considerably smaller than the 27.1m of the reference aircraft due to the lower slenderness ratio of the tail cone that was chosen, the low seat pitch that was selected, and the fact that luggage and cargo are assumed to be stowed below the passenger floor. The quarter-chord point of the mean aerodynamic chord (MAC) is located at 46.5% of the fuselage length, which is a little aft of the reference value of 43%.

While all three aircraft fulfill the same set of requirements, their key performance indicators differ substantially, as is shown in Table 2. The two aircraft with aft-mounted propulsions systems show an increase in maximum takeoff mass of 1.0 and 0.8 metric tonnes, respectively. The TMP aircraft has the highest increase in weight, due to the increased mass of the fuselage and horizontal tail plane. However, due to its more favorable CG position at its maximum zero-fuel weight it has less trim drag and therefore burns less fuel compared to the TMDP aircraft.

The harmonic mission sizes each of these aircraft. The obtained mission profiles are shown in Figure 9 and show overall similarity between the three different configuration except for the climb

Table 2 Key performance indicators for the three synthesized aircraft

Parameter	Unit	WMP	TMP	FMDP
MTOM	t	22.9	23.7	23.7
OEM	t	13.2	13.8	13.7
Mission fuel	t	2.2	2.3	2.5
Power loading	N/kW	63.7	63.5	63.0
Wing loading	N/m^2	3330	3340	3350
$X_{\bar{c}/4}/L_{\text{fus}}$	-	0.47	0.49	0.52

profile which is dictated by a predefined split of excess power between acceleration and climb. The time-to-climb requirement of 17.5 minutes is not reached due to a lack in excess power. It can be observed that the harmonic mission is completed after approximately 3 hours and 10 minutes.

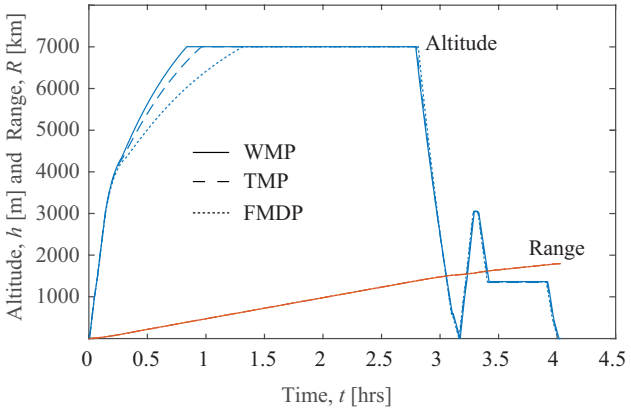

Fig. 9 Resulting mission profiles for each of the three synthesized aircraft configurations: Wing-mounted propellers (WMP), tail-mounted propellers and fuselage-mounted ducted propellers (FMDP).

While the on-design mission performance is virtually identical for all aircraft, the payload-range diagram shown in Figure 10 shows that the off-design mission performance differs between the three configurations. Due to the superior aerodynamic performance, the WMP aircraft has the highest off-design range, regardless of the payload weight, the TMP comes in second, while the FMDP has the lowest off-design range. It should be noted that each of these aircraft is sized with a fuel tank spanning up to 80% of their relative wing span. As the TMP and FMDP have a 4% larger wing area, their fuel tank is about 5% larger then for the WMP. So even as they can carry more fuel, their off-design mission range is still lower than for the WMP. This attributed to two factors: weight and friction drag. Due to the increased operating empty weight, the induced drag is higher at any point in the cruise flight. Furthermore, the larger minimum drag coefficient stemming from the increase in wetted area also increases the parasite drag of the aircraft. As a result, the WMP aircraft has the best off-design mission performance.

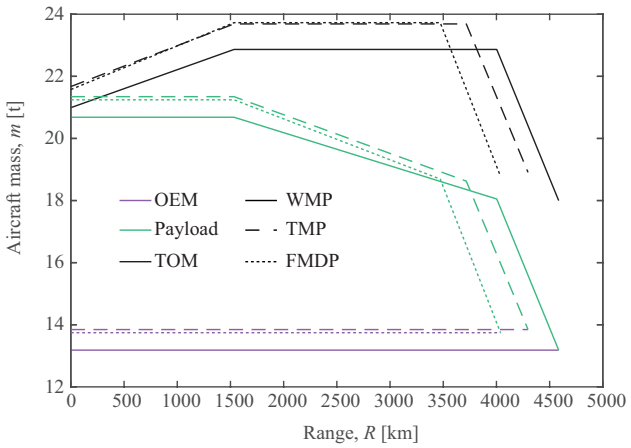

Fig. 10 Comparison of the payload-range diagrams for the three different aircraft. TOM is take-off mass, OEM is operational empty mass.

5 Conclusions

Two innovative aircraft configurations featuring tail-mounted propeller and fuselage-mounted, ducted propellers have been assessed in terms of their key performance indicators assuming they are designed for a harmonic mission of 1530km and 68 passengers. A conventional aircraft with wing-mounted propellers has been designed as a reference case and showed very comparable characteristics to the ATR-72-600 in terms of geometry and weight. It has been shown that the two innovative configurations can be designed to the same top-level aircraft requirements as the conventional aircraft and that these designs could be feasible in terms of stability, balance, and

point performance. The innovative aircraft are expected to see an increase in maximum take-off mass of 3%, an increase in operating empty mass up to 5%, and an increase in fuel burn up to 12% over the harmonic mission. Each of these changes has been attributed to the large center-of-gravity excursion during loading that is caused by the aft location of the propulsion system for these innovative configurations. While the aircraft with ducted propellers showed the least favorable results, its drag estimates were fairly conservative and the beneficial interaction between fan and duct were not yet taken into account. This could offset some of the drag increases reported herein and make the ducted propeller a viable alternative to the wing-mounted propeller configuration.

References

[1] BOUQUET, T., AND VOS, R. Modeling the propeller slipstream effect on lift and pitching moment. In *Proceedings of the 2017 AIAA Aerospace Sciences Meeting* (Grapevine ,TX, 2017).

[2] ELMENDORP, R., VOS, R., AND LA ROCCA, G. A conceptual design and analysis method for conventional and unconventional airplanes. In *Proceedings of the 29th Congress of the International Council of Aeronautical Sciences* (St. Petersburg, Russia, 2014).

[3] GOLDSMITH, I. M. A study to define the research and technology requirements for advanced turbo/propfan transport aircraft. Tech. rep., 1981.

[4] HARINARAIN, V. Aerodynamic performance study on ducted propeller system for propulsion and control and stability applications. Master's thesis, 2017.

[5] NICOLOSI, F., CORCIONE, S., TRIFARI, V., CUSATI, V., RUOCCO, M., AND DELLA VECCHIA, P. Performance evaluation and doc estimation of an innovative turboprop configuration. In *Proceedings of the 2018 Aviation Technology, Integration, and Operations Conference* (Atlanta, GA, 2018).

[6] RAYMER, D. P. *Aircraft Design: A Conceptual Approach*. AIAA, 2012.

[7] ROSKAM, J. *Airplane Design*. DAR corporation, 1986.

[8] SCHUT, J., AND VAN TOOREN, M. Design "feasilization" using knowledge-based engineering techniques. *Journal of Aircraft 44* (2007), 1776–1786.

[9] TORENBEEK, E. *Synthesis of Subsonic Airplane Design*. Delft University Press, 1982.

[10] WEISSINGER, J. Zur aerodynamik des ringfluegels. die druckverteilung duenner, fast drehsymmetrischer fluegel in unterschallstroemung. *Zeitschriftfiir Flugwissenschaften 4* (1956), 141.

Acknowledgements

The authors would like to acknowledge the contribution of ir. Tom Schouten, ir. Vikesh Harinarain, and ir. Malcom Brown whose work was used to generate the results presented in this paper.

Contact Author Email Address

Corresponding author:
Roelof Vos; R.Vos@tudelft.nl

Copyright Statement